dark-yellow, non-adherent oxide forms on the metal surface.

A consideration of data[1] on the rate of corrosion in different concentrations of formic acid at 35° C. reveals that zone *C* corresponds to the range of concentration where the corrosion-rate is high and region *A* where the corrosion-rate is at a minimum.

It is apparent that the mechanism of micropitting is highly complex, as the electrode processes which occur involve the anodic oxidation of titanium, localized corrosion of titanium, oxidation of formic acid to carbon monoxide and dioxide and oxidation of hydroxyl to oxygen. The heterogeneity of the metal and adsorption of formic acid on active centres[2,3] and the formation of complexes between titanium and formic acid may also contribute to the overall process.

The reason for the formation of barrier films at more elevated temperatures and at higher acid concentrations (Fig. 1, zone *A*) may involve a consideration of the kinetics of oxidation of formic acid and the properties of the anodic oxide film under the conditions specified.

The phenomenon of micropitting appears to be confined to the titanium–formic acid system as similar results could not be achieved with niobium or zirconium.

It is considered that further work on this phenomenon may contribute to an understanding of the general mechanism of the pitting corrosion of metals.

The anodizing of titanium in formic acid to produce a micropitted surface as an aid to anti-galling, lubrication and adhesion of surface coatings is covered by a patent application[4] made by the National Research Development Corporation.

R. A. Piggott
L. L. Shreir

Metallurgy Department,
Battersea College of Technology,
London, S.W.11.

[1] Lane, I. R., Golden, L. B., and Ackerman, W. L., *Indust. Eng. Chem.*, **45**, 1067 (1953).
[2] Müller, E., *Z. Elektrochem.*, **33**, 561 (1927).
[3] Herasymenko, P., *Ukrainskii Kem. Zhur.*, **4**, Sci. Pt., 439 (1929).
[4] B.P. App. No. 19688/59 and 53/60.

Some New Intermetallic Compounds of Thorium of the Type Th_7X_3

As part of an investigation of the constitution of alloys of thorium with the metals ruthenium, rhodium, palladium, osmium, iridium and platinum, a series of 1-gm. samples of alloys containing up to 33 atomic per cent of each precious metal was prepared by arc-melting the component materials in a zirconium-gettered argon atmosphere, weight losses on melting being negligible. Metallographic and X-ray results on as-cast and on annealed material suggest that the intermetallic compounds richest in thorium are: Th_7Ru_3, Th_7Rh_3, Th_2Pd, Th_7Os_3, Th_7Ir_3 and Th_7Pt_3. Each compound forms a eutectic with thorium and the composition and temperature of these eutectics are given in Table 1. The solid solubility of each metal in thorium and the age-hardening behaviour of thorium-rich alloys have also been investigated.

Alloys corresponding to the five compounds, Th_7X_3, were brittle and powders for X-ray studies were prepared by crushing in air; powder patterns were obtained with a Guinier-type focusing camera using monochromatized copper radiation. These X-ray

Table 1

System	Phases in the eutectic	Composition of the eutectic (percentage of precious metal)	Melting point of the eutectic (deg. C.)
Th – Ru	Th + Th_7Ru_3	16 ± 1	1,262 ± 12
Th – Rh	Th + Th_7Rh_3	20 ± 1	1,237 ± 12
Th – Pd	Th + Th_2Pd	22 ± 1	1,112 ± 12
Th – Os	Th + Th_7Os_3	14 ± 1	1,287 ± 12
Th – Ir	Th + Th_7Ir_3	15 ± 1	> 1,300
Th – Pt	Th + Th_7Pt_3	17·5 ± 0·5	1,242 ± 12

Table 2

Compound	'a' (Å.)	'c' (Å.)	c/a	X-ray density (gm./c.c.)
Th_7Ru_3	9·969	6·302	0·632	11·82
Th_7Rh_3	10·031	6·287	0·627	11·71
Th_7Os_3	10·031	6·296	0·628	13·27
Th_7Ir_3	10·076	6·296	0·625	13·40
Th_7Pt_3	10·126	6·346	0·627	13·01

films were indexed on the basis of a hexagonal lattice, systematic extinctions of the $h\,h\,\overline{2h}\,l$ reflexions were noted when l was odd and the observed intensities show good agreement with those for the Th_7Fe_3 structure, space group $C^4{}_{6V} - P\,6_3mc$. Lattice parameters, axial ratios and X-ray densities for the new compounds are given in Table 2.

Grateful acknowledgment is made to Prof. J. G. Ball under whose supervision this work was carried out, and also to the Atomic Energy Research Establishment, Harwell, for financial support and for allowing me to make use of some experimental facilities.

J. R. Thomson*

Department of Metallurgy,
Imperial College of Science and Technology,
London, S.W.7.

* Formerly J. R. Murray.

CRYSTALLOGRAPHY

X-Ray Correlation of the *A-B* Layer Order of Cadmium Selenide with the Sign of the Polar Axis

Cadmium selenide (CdSe) is typical of the hexagonal semiconducting compounds formed from elements of Group II and Group VI of the Periodic Table. It possesses the wurtzite structure and contains a unique polar axis (the *c*-axis). Compression along this axis produces opposite electric charges on the basal faces, which also differ in their response to etching and in other properties. An examination of the crystal structure as shown in Fig. 1 shows the polarity clearly. Viewed normal to the *c*-axis, pairs of closely spaced cadmium–selenium layers are seen. The 'cadmium side' and the 'selenium side' are defined in Fig. 1.

For an understanding of the polar physical and chemical effects it is important to know which is the cadmium and which is the selenium side of the *c*-axis. It is possible to make such an identification by observing the effects of anomalous X-ray dispersion on the intensity of the X-rays reflected from the positive and negative sides of the basal planes (00.*l*) and (00.$\bar{l}$). Previous workers have investigated cubic zinc sulphide, gallium arsenide and indium arsenide in such a manner[1–3]. To our knowledge, this communication reports the first application of this

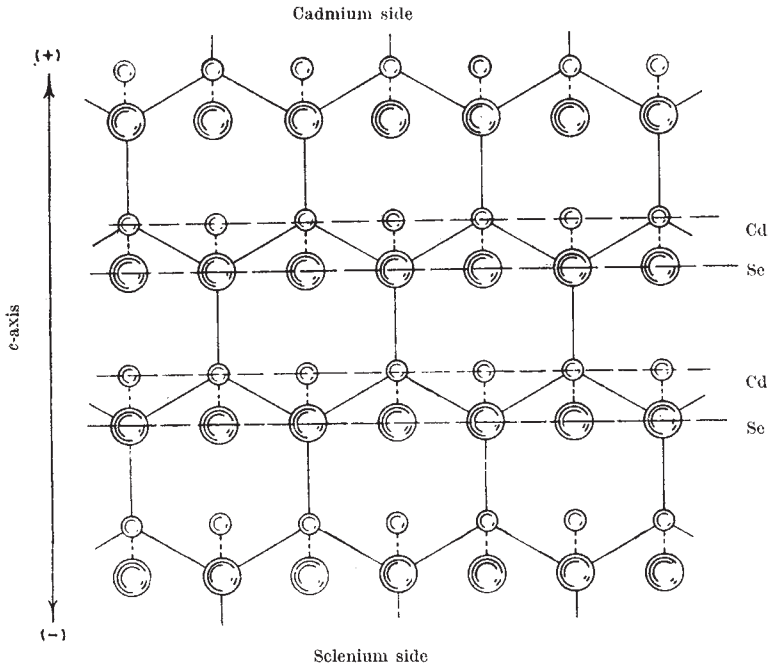

Fig. 1. Alternate layers of cadmium and selenium parallel to the (00.1) surfaces

technique to a wurtzite structure. By making dispersion corrections to the atomic scattering factor, the structure factor ratio $\frac{|F(00.l)|^2}{|F(00.\bar{l})|^2}$ (which is proportional to the ratio of the integrated intensities) can be calculated[4]. These theoretical ratios calculated for copper $K\alpha$ radiation are shown in Table 1.

Table 1. Rotated Integrated Intensity Ratios

Plane	Theoretical intensity ratio $\frac{\lvert F(00.l)\rvert^2}{\lvert F(00.\bar{l})\rvert^2}$	Observed intensity ratio
00.2	0·869	0·862
00.4	1·000	0·973
00.6	1·225	1·241
00.8	1·000	1·045

The experimental procedure is quite exacting. A circular plate of cadmium selenide, the surface of which was orientated to within 3 min. of arc with the (00.1) plane, was etched and given an optical polish with 0·3μ alumina. Measurements with an optical flat indicate that both surfaces were slightly rounded but were flat to 10 fringes. Next, the disk was placed on a bed of wax in a cylinder which was inserted into the rotating flat specimen spinner of a standard 'Norelco' diffractometer. The polished crystal was pushed up against an optical flat which was held against the top surface of the specimen holder. When the interference rings were centred, the crystal was locked into position. To test the parallelism of the crystal surface with the plane of the specimen holder, the latter was rotated by motor while a distant light source was reflected off the rotating crystal surface. The steadiness of this optical image proved to be an extremely sensitive test of the line-up. The experimental values for the integrated intensities were obtained by counting while simultaneously rotating the crystal at 77 r.p.m. and slowly scanning the entire peak at 1/8° (2θ) per min. After the rotated integrated intensities were measured on one side, the crystal was turned over, aligned, and the same process was repeated (care being taken that all conditions were identical for any two (00.l) (00.$\bar{l}$) reflexions). For different peaks various aluminium filters were used so that the counting-rate fell within the linear response range of the scintillation counter. Table 1 compares a typical set of results with the corresponding theoretical values.

The side of the crystal proved to be the cadmium side by the X-ray data of Table 1 was found to become positively charged on extension. By the sign convention of the I.R.E. 1949 Standard on Piezoelectricity the + end is therefore the outward directed normal from the cadmium side.

Having established this correlation, other differentiating properties of opposite (00.1) surfaces which have been correlated to the piezoelectric sign can also be related to the A–B layer order. Table 2 is a tabulation of some of these correlations for cadmium selenide.

Considering the similar character of all wurtzite and sphalerite compounds, it would appear reasonable for these compounds to show the same type of correlation as cadmium selenide, namely, the more metallic layer will be in the $+c$ direction, as defined by the piezoelectric sign. This is in keeping with the findings for zinc sulphide and (by inference from the etching behaviour) for gallium arsenide and indium arsenide[1–3]. Any theory which attempts to explain the differentiating properties of the opposite (00.1) surfaces of wurtzite and the opposite (111) surfaces

Table 2. Correlation of $A-B$ Layer Order with Other Properties which Distinguish the Opposite (00.1) Surfaces of Cadmium Selenide

Property	(00.1) surface. Outward normal to surface points in $+c$ direction	(00.1) surface. Outward normal to surface points in $-c$ direction
Sign of piezoelectricity on extension	(+) As defined by 1949 I.R.E. convention	(−)
$A-B$ layer order	See Fig. 1	
Etching characteristics in aqua regia (excess selenium removed)	Shiny, symmetric pits bevelled edges. Equal or slower etch rate	Dull or cratered, no symmetry pits, no edge bevelling. Equal or faster etch rate
Relative sign of electrolytic solution potential 1 : 1 aqua regia	(+) More 'noble' by 50–70 mV.	(−)
Crystal habit at positive and negative ends	More complex pyramid development	Prominent face is the pedion. Pyramids small or absent

for sphalerite compounds must be compatible with these findings.

This work was supported by the U.S. Air Force, Wright Air Development Division.

R. Zare
W. R. Cook, jun.
L. R. Shiozawa

Clevite Corporation,
540 East 105 St.,
Cleveland 8,
Ohio.

[1] Coster, D., Knol, K. S., and Prins, J. A., *Z. Phys.*, **63**, 345 (1930).
[2] White, J. G., and Roth, W. C., *J. App. Phys.*, **30**, 946 (1959).
[3] Warekois, E. P., and Metzger, P. H., *J. App. Phys.*, **30**, 960 (1959).
[4] Dauben, C. H., and Templeton, D. H., *Acta Cryst.*, **8**, 842 (1955).

OCEANOGRAPHY

Organic Acids in Pacific Ocean Waters

Organic acids dissolved in waters of the Pacific Ocean were isolated by : (1) solvent extractions with carbon disulphide and chloroform, and (2) by co-precipitation with ferric hydroxide sols.

The solvent extractions were carried out on 15·3–20·0 l. of sea-water samples freed of particulate matter by filtration through '*HA* Millipore' filters (pore size : 0·45μ). The residues from chloroform and carbon disulphide extracts were methylated with methanol and a trace of concentrated sulphuric acid, and these products were then submitted to gas chromatographic analysis using an 'Aerograph' model 110-*C* gas chromatograph (Wilkens Instrument Co., Walnut Creek, California) incorporating 5- and 10-ft. Craig polyester succinate columns. The fatty acid esters isolated were identified by their retention times on the column with respect to known fatty acid esters and in the case of the methyl esters of palmitic and stearic acids by collection from the column and subsequent infra-red spectra. Table 1 lists the fatty acids isolated in μgm./l., and includes pertinent data on sample location and depth, extraction *p*H, and indicates the amounts of the unknown fatty acids C_x, C_y and C_z. From their infra-red spectra, C_x, C_y and C_z are indicated to be fatty acid esters. Their relative positions on the gas chromatographic traces gave retention times identical with the C_{15}, C_{17} and C_{19} normal, saturated fatty acid esters. Fig. 1 illustrates two representative traces for samples 47-*A* and 10-*A*.

To determine the percentage recovery of the fatty acids from sea-water a tracer experiment was run using palmitic acid-1-^{14}C (Nuclear-Chicago, Cat. No. *CFA*-23), added as 2,345 c.p.m. to each 2·40–2·48 l. sample of filtered sea-water prior to extraction with chloroform. The samples were acidified with hydrochloric acid to a *p*H of 2·0, and the solvent

Table 1. Fatty Acids isolated from Sea-water

Sample (1)	Location	Depth collected (m.)	Depth to bottom (m.)	Volume extracted (l.)	Extraction (*p*H)	μgm./l.												Miscellaneous	No. of major peaks (5)	Total (μgm./l.) (3)
						Saturated						Unsaturated Mono-	Unsaturated di-	Unknown						
						C_{12}	C_{14}	C_{16}	C_{18}	C_{20}	C_{22}	C_{16} (C=C)	C_{18} (C=C)	C_{18} (C=C)$_2$	C_x	C_y	C_z			
10*A*	31° 40′ N. 119° 35′ W.	1,000	3,290	19·0	1·30	2·3	4·3	20·9	14·2	1·8	1·4	0·3	8·3	1·4	—	—	—	1·6 (4)	13	56·5
55*A**	32° 40′ N. 118° 09′ W.	1,200	2,020	18·1	3·10	0·4	1·8	14·6	22·2	8·1	tr.	—	—	—	6·6	15·5	14·1	6·4	14	89·7
47*A**	32° 40′ N. 118° 09′ W.	1,500	2,020	19·0	2·88	0·2	1·3	7·9	14·0	7·0	tr.	—	—	—	3·3	10·1	9·2	7·4	14	60·4
127*B*	25° 19′ N. 114° 05′ W.	1,957	4,070	20·0	2·30	0·3	2·5	12·2	17·7	5·4	—	—	—	—	6·2	13·1	10·1	4·2	14	71·7
34*A*	46° 46′ S. 123° 57′ W.	2,427	4,330	15·4	2·23	1·5	1·6	3·2	7·1	tr.	—	—	—	—	tr.	tr.	tr.	6·7	10	20·1
37*A*	26° 45′ N. 123° 00′ W.	987	4,280	20·0	7·50	0·7	2·9	11·1	8·9	2·5	—	0·8	1·4	1·0	—	—	—	3·6	10	32·9
24*A*	31° 41′ N. 119° 35′ W.	1,020	3,570	19·0	7·50	0·5	1·9	8·3	6·5	1·5	—	3·0	7·5	2·9	—	—	—	0·1	10	32·2
35*A*	46° 46′ S. 123° 57′ W.	2,427	4,330	15·3	7·58	0·3	0·4	2·7	—	—	—	—	—	—	—	—	—	—	7	3·4
70*C* (2)	32° 40′ N. 118° 09′ W.	1,500	2,020	56	4·5	0·3	0·5	1·5	3·7	2·1	tr.	—	—	—	1·0	2·0	2·5	2·7	10	16·3

(1) Samples marked with asterisk were extracted with carbon disulphide; samples not marked, with chloroform.
(2) This sample had previously been precipitated with ferric hydroxide.
(3) These values represent minimum yields and are felt to be correct within a factor of two.
(4) Appears to be palmitolinoleic (hexadecadienoic) ester. Also shows indications of C_{16} and the unsaturated analogues of C_{12} and C_{14}.
(5) Identifiable peaks appearing on the gas chromatographic traces.

Table 2. Palmitic Acid-1-^{14}C Tracer Experiment

Sample (1)	Depth (m.)	Volume (l.)	Percentage of recovery free acid	Percentage of recovery methyl esters	Acids isolated as methyl esters (μgm./l. water) (3)							
					C_{12}	C_{14}	C_{16}	C_{18}	C_{16} (C=C)	C_{18} (C=C)	C_{18} (C=C)$_2$	Total
Control (2)	—	2·40	75·7	13·0	3·3	4·4	6·6	—	—	—	—	14·3
1	10	2·48	97·9	8·9	1·9	3·3	24·8	—	—	—	—	30·0
2	91	2·44	96·4	12·5	4·1	5·0	28·5	7·5	18·2	11·1	10·2	84·6
3	460	2·44	96·4	10·9	2·7	3·9	17·4	14·5	8·7	11·4	11·7	70·3
4	924	2·40	98·1	14·0	1·8	6·8	41·0	16·5	3·5	34·8	17·3	111·7
5	1,388	2·45	90·0	19·1	2·0	5·6	18·2	25·6	—	—	—	51·4
6	1,853	2·47	91·6	9·8	—	—	30·4	—	—	—	—	30·4
7	2,491	2·40	80·5	5·2	—	—	35·8	—	—	—	—	35·8
8	2,665	2·42	81·2	6·1	—	13·9	19·1	—	—	—	—	33·0

(1) Location : 30° 23·4′ N. ; 119° 13′ W. Depth to bottom : 3,660 m.
(2) 40l. of double-distilled water previously found to contain traces of fatty acids.
(3) Corrected to 100 per cent yield on the basis of the percentage recovery of the methyl esters.